Environmental Technology & Innovation 43 (2026) 105048

Contents lists available at ScienceDirect

Environmental Technology & Innovation

journal homepage: www.elsevier.com/locate/eti

Microwave-assisted activated carbon from waste compressed wood for efficient PFOS removal under neutral pH conditions

Mona Ardebilipour [a], Mahdi Maleki Lonbar [a], Ghufran Redzwan [b], Majid Baghdadi [a,*]

[a] Faculty of Environment, Department of Environmental Engineering, University of Tehran, Tehran, Iran
[b] bInstitute of Biological Sciences, University of Malaya, Kuala Lumpur, Malaysia

ARTICLE INFO

Keywords:
Perfluorooctanesulfonic acid (PFOS)
Microwave-assisted activated carbon
Biomass-derived adsorbent
Emerging contaminants
Water treatment

ABSTRACT

Perfluorooctanesulfonic acid (PFOS) is a persistent fluorinated contaminant that presents serious challenges for water treatment due to its chemical stability and mobility. In this study, a sustainable activated carbon was synthesized from discarded compressed wood through phosphoric acid impregnation followed by microwave assisted activation. Response surface methodology was applied to optimize both the synthesis conditions and the adsorption process. The optimized synthesis produced an adsorbent with a high specific surface area of 1226 $m^2 g^{-1}$, well developed mesoporosity, and abundant oxygen and phosphorus containing surface functionalities. Adsorption optimization identified a contact time of 4.82 h, adsorbent dosage of 1.95 $g L^{-1}$, and natural solution pH of 7.0 as the optimal operating conditions, achieving a PFOS removal efficiency of 97.87 % at an initial PFOS concentration of 5 $mg L^{-1}$. Adsorption equilibrium was best described by the nonlinear Langmuir isotherm with a maximum adsorption capacity of 60.85 $mg g^{-1}$, while adsorption kinetics followed a pseudo second order model, indicating surface controlled interactions. The adsorbent also exhibited excellent regeneration performance, maintaining more than 95 % of its removal efficiency after multiple reuse cycles. The combination of waste derived precursor utilization, rapid microwave assisted synthesis, high removal efficiency under neutral pH conditions, and strong reusability highlights the potential of this material as a practical and scalable adsorbent for PFOS remediation in water and wastewater treatment systems.

1. Introduction

The extensive production and use of per- and polyfluoroalkyl substances (PFAS) over the past several decades have resulted in their pervasive distribution across environmental matrices. Perfluorooctane sulfonate (PFOS) is a synthetic fluorinated contaminant whose chemical stability and bioaccumulation potential pose significant environmental and toxicological risks (Taghizad et al., 2025; Yang et al., 2025). As a result, PFOS has been classified as a persistent organic pollutant (POP) under the Stockholm Convention, and regulatory agencies in many regions have implemented stringent limits for PFOS concentrations in water.

The environmental persistence of PFOS necessitates the development of treatment methods that are both high-performing and operationally sustainable. A variety of physical, chemical, and biological treatment technologies have been investigated for PFOS

* Corresponding author.
E-mail addresses: mona.ardebilipour@ut.ac.ir (M. Ardebilipour), mahdimalekilonbar@ut.ac.ir (M.M. Lonbar), ghufran@um.edu.my (G. Redzwan), m.baghdadi@ut.ac.ir (M. Baghdadi).

https://doi.org/10.1016/j.eti.2026.105048
Received 4 January 2026; Received in revised form 10 May 2026; Accepted 11 June 2026
Available online 12 June 2026

remediation. Membrane-based processes such as nanofiltration and reverse osmosis can efficiently separate PFOS; however, they generate concentrated reject streams requiring further management, which shifts rather than resolves the contamination problem (Lee et al., 2022; Ma et al., 2024). Several oxidative and reductive processes including advanced oxidation processes, electrochemical degradation, and photocatalysis struggle to mineralize PFOS due to the high stability of its fluorinated tail and may generate partially defluorinated intermediates that pose additional risks (Chen et al., 2024; Juve et al., 2024; Zhang et al., 2024). Ion-exchange resins and molecularly imprinted polymers offer strong selectivity but are relatively expensive, sensitive to fouling, and often unsuitable for large-scale deployment (Boyer et al., 2021).

These limitations have positioned adsorption as one of the most promising and pragmatic technologies for PFOS removal. Adsorption offers several key advantages: operational simplicity, low energy requirements, broad applicability to varying water matrices, and the ability to remove PFOS even at trace environmental concentrations. Importantly, adsorption does not produce harmful transformation products, and many adsorbents can be regenerated and reused, contributing to economically and environmentally sustainable treatment schemes (Ao et al., 2024; Cheng et al., 2024; Yavari et al., 2025).

Activated carbon (AC) remains the benchmark adsorbent for PFOS remediation and adsorbs PFOS through several complementary mechanisms, including hydrophobic interactions, electrostatic attraction, and pore-filling within the porous network (Khedri et al., 2022; Nobakht et al., 2023). The highly fluorinated carbon chain makes the molecule strongly hydrophobic, which promotes its association with non-polar domains on the carbon surface (Liu et al., 2024; Vatankhah et al., 2024). Depending on solution pH and surface functional groups, charged sites at the adsorbent interface can also contribute to electrostatic attraction between positively charged surface species and the anionic sulfonate headgroup of PFOS. In addition, PFOS molecules can be physically retained within micro- and mesopores, so that pore-filling operates in parallel with surface interactions (Hassan et al., 2022; Lee et al., 2023). For PFAS containing aromatic moieties, π–π interactions with graphitic domains on the carbon surface may further stabilize adsorption, whereas for PFOS, hydrophobic interactions, electrostatic attraction, and pore-filling are generally considered the dominant mechanisms. The synergy of these mechanisms enables activated carbon to efficiently capture PFOS across a wide range of concentrations and water matrices (Choudhary et al., 2022; Zhang et al., 2021).

The activation process plays a critical role in determining the structural and chemical characteristics of activated carbon and, consequently, its adsorption performance. During activation, whether by physical or chemical routes, the carbon matrix develops an extensive network of micro- and mesopores and a much higher specific surface area, providing a larger number of accessible sites for adsorbing contaminants such as PFOS (Huang et al., 2024; Pauletto et al., 2023; Yang et al., 2021). Traditional furnace-based thermal activation typically requires long heating durations and high energy input and often produces relatively non-uniform pore development with limited control over pore-size distribution. In contrast, microwave-assisted activation has gained increasing attention because rapid volumetric heating and shorter processing times improve energy efficiency and promote the formation of more homogeneous and accessible pore structures (Kalinke et al., 2023; Wu et al., 2025). When combined with chemical activating agents such as phosphoric acid, microwave heating can generate highly porous carbons enriched with oxygen- and phosphorus-containing surface functionalities. The resulting combination of tailored pore architecture and modified surface chemistry strengthens the key adsorption mechanisms governing PFOS uptake, including hydrophobic interactions with the fluorinated carbon backbone, electrostatic attraction between charged surface sites and the anionic sulfonate headgroup, and pore-filling within micro- and mesopores (Abdelsamad et al., 2025; Pauletto et al., 2022).

However, the performance of commercial AC can be significantly affected by natural organic matter competition and the high production costs associated with conventional activation (Norouzi et al., 2020; Zahed et al., 2022). Consequently, considerable research has focused on developing low-cost, biomass-derived activated carbons that provide comparable performance with improved economic and environmental profiles. Biomass waste streams, including agricultural residues and lignocellulosic by-products, offer abundant raw materials for AC production while also reducing waste-disposal burdens (Mollasalehi et al., 2026). Compressed wood, widely produced in the furniture industry, is often discarded after short-term use or burned as fuel, contributing to environmental pollution (Bosch et al., 2022). Despite its availability, compressed wood remains an underutilized precursor for converting waste materials into value-added activated carbon suitable for water treatment applications (Jjagwe et al., 2021).

While biomass-derived activated carbons have been widely explored, a critical operational bottleneck persists in the literature: the predominant requirement for acidic environments to facilitate effective perfluorooctanesulfonic acid (PFOS) capture via electrostatic interactions. To address this technical gap, the present study investigates the rapid microwave-assisted synthesis of activated carbon utilizing discarded compressed wood as a sustainable, zero-cost precursor. This research establishes a novel pathway for developing high-surface-area (1226 $m^2\ g^{-1}$) adsorbents that utilize a multimodal mechanism—comprising hydrophobic partitioning, pore-filling, and heteroatom-mediated interactions—to achieve superior PFOS removal efficiency (97.9%) under environmentally relevant neutral pH conditions (7.0). By optimizing the synthesis parameters via response surface methodology (RSM), we demonstrate that the integration of microwave heating and phosphoric acid activation produces an adsorbent with unique hierarchical porosity and phosphorus-containing functionalities that circumvents the need for intensive chemical pH adjustment. Ultimately, this work provides a scalable and energy-efficient strategy for PFOS remediation, addressing both waste management challenges and the practical requirements of real-world water treatment systems.

2. Materials and methods

2.1. Materials

PFOS (CAS No. 1763–23–1) was sourced from Sigma-Aldrich. Phosphoric acid (H_3PO_4, 85% w/w), ethanol (C_2H_6O, 96% v/v),

sodium hydroxide (NaOH), and hydrochloric acid (HCl, 37% w/w) were supplied by Merck (Germany). Compressed wood derived from discarded furniture was collected from the University of Malaya dumping site.

2.2. Raw material preparation

The discarded compressed wood was first ground using a rapid granulator (Germany) to reduce its size and ensure uniform processing. The ground material was then sieved to obtain particles in the 1–2 mm range. To ensure the removal of surface impurities and organic dust, the sieved compressed wood was subjected to exhaustive washing with deionized water until the supernatant reached a stable turbidity level. The precursor was then dried to a constant weight in a forced-air oven at 105°C for 24 h. This rigorous drying stage was essential to ensure that residual moisture did not interfere with the calculated phosphoric acid impregnation ratio during the chemical activation phase. The dried precursor was then stored in sealed containers until use in the activation process.

2.3. Synthesis of activated carbon

Activated carbon was synthesized through chemical activation using phosphoric acid. A total of 20 g of the dried precursor was mixed with 40% (v/v) H_3PO_4 and allowed to impregnate for 3–4 h. The impregnated material was then dried at 105–110 °C for 24 h. The dried precursor was weighed and transferred to a quartz reactor for activation using a microwave heating system (Synotherm, France). The activation process was conducted in a specialized quartz reactor within the Synotherm microwave system. The device was operated at the selected power and duration while maintaining a continuous ultra-high purity nitrogen flow of 400 mL min^{-1}. This flow rate was precisely optimized to ensure the rapid evacuation of volatile devolatilization products, thereby preventing secondary char formation and ensuring an inert reaction environment. This constant nitrogen stream ensured an inert reaction environment and was maintained at 400 mL min^{-1} to facilitate the rapid evacuation of devolatilization byproducts. High flow rates are essential during microwave-assisted activation to prevent secondary char formation and the subsequent blocking of nascent pores, which can occur due to the rapid release of volatiles during accelerated volumetric heating.

Following microwave activation, the produced activated carbon was thoroughly rinsed with distilled water until the wash water reached neutral pH. This washing stage is essential for removing residual phosphoric acid from within the pore network, which facilitates the development of porosity and enhances adsorption efficiency (Thue et al., 2016). The washed samples were subsequently dried in an oven at 105°C until a stable weight was obtained, ensuring complete moisture removal. The final dried activated carbon was then stored in sealed containers for subsequent characterization and adsorption experiments.

To determine the optimal activation conditions, response surface methodology (RSM) was applied to synthesize activated carbon with suitable structural characteristics for PFOS adsorption. A central composite design (CCD) consisting of 18 experimental runs was used to evaluate the effects and interactions of the key synthesis variables, namely the impregnation ratio, microwave power, and activation time. This design enabled simultaneous assessment of linear, quadratic, and interaction terms while minimizing the number of experiments required for statistically robust modeling. The resulting predictive equations described the relationship between synthesis parameters and adsorbent performance and were used to identify the activation conditions expected to produce the most effective carbon material.

2.4. Characterization

The physicochemical properties of the activated carbon were examined using standard analytical techniques. Surface morphology and elemental distribution were analyzed by field-emission scanning electron microscopy (FESEM) coupled with energy-dispersive X-ray spectroscopy (EDS mapping) using a MIRA3 system (TESCAN, Czech Republic). The specific surface area and pore characteristics were determined via the Brunauer–Emmett–Teller (BET) method using a BELSORP MINI II analyzer (BEL, Japan). Functional groups were identified using Fourier transform infrared (FTIR) spectroscopy (AVATAR, Thermo Scientific, USA) over the 400–4000 cm^{-1} range. Raman spectroscopy (TakRam N1–541, TakRam, Iran) was used to evaluate structural order and defect characteristics of the carbon matrix.

2.5. Batch adsorption experiments

Batch adsorption tests were carried out in 250 mL glass beakers, each containing 50 mL of PFOS solution. The pH of the solution was regulated using sodium hydroxide (NaOH) and hydrochloric acid (HCl) at concentrations of 0.1 and 1 mol L^{-1} . Measured amounts of the adsorbent were then introduced to initiate the adsorption process. The mixtures were kept under constant stirring for specified time intervals to ensure uniform contact. After the designated contact time, the suspensions were sampled and the residual PFOS concentration was determined by LC–MS/MS. PFOS removal performance was expressed as percentage removal and calculated according to Eq. (1):

$$Removal\ (\%) = \frac{C_i - C_e}{C_i} \times 100 \quad (1)$$

Where C_i(mg L^{-1}) represents the initial PFOS concentration and C_e(mg L^{-1}) denotes its concentration at equilibrium. All experiments were conducted in duplicate, and the values presented correspond to the average results.

2.6. PFOS analysis

The concentration of PFOS was measured using liquid chromatography coupled with tandem mass spectrometry (LC-MS/MS; Quattro Micro API, Micromass Waters 2695). The performance of the LC-MS/MS method was validated to ensure proper sensitivity and precision. The limit of detection (LOD) was found to be 0.5 μg L−1 (S/N = 3), and the limit of quantification (LOQ) was 1.7 μg L−1 (S/N = 10), based on signal-to-noise (S/N) ratios from PFOS standards prepared in ultrapure water. To assess potential matrix effects, PFOS-fortified tap water and groundwater samples were analyzed under the same conditions, yielding recoveries between 91% and 104%. These results indicated minimal matrix interference, confirming that the LC-MS/MS method offered sufficient sensitivity and accuracy for all PFOS concentrations used in the adsorption experiments.

2.7. Removal process optimization

RSM was further employed to optimize the operational parameters governing PFOS removal during adsorption. A central composite design comprising 29 experimental runs was used to investigate the combined effects of solution pH, initial PFOS concentration, adsorbent dosage, and contact time. The selection of synthesis and adsorption parameter ranges was informed by preliminary screening experiments designed to identify the operational boundaries between insufficient activation and structural degradation. For the synthesis phase, the impregnation ratio (1.0–3.0), microwave power (500–1000 W), and activation time (10–20 min) were chosen to span the transition from partial carbonization to excessive etching, ensuring the identification of a true global optimum for pore development. Similarly, the adsorption parameter ranges including pH (3–10), adsorbent dosage (0.2–2 g L^{-1}), and initial concentration (5–50 mg L^{-1}) were defined to encompass environmentally relevant conditions while providing sufficient data for the robust capture of non-linear interaction effects. Optimal operational conditions were selected based on maximized removal efficiency and the statistical significance of the fitted model, ensuring reliable identification of effective adsorption settings (Kangani et al., 2024; Lonbar et al., 2025).

2.8. Isotherm and kinetic modeling

Adsorption equilibrium studies were performed to evaluate the interaction between PFOS and the synthesized activated carbon. The experimental data were fitted using both linear and nonlinear forms of the Langmuir, Freundlich, and Temkin isotherm models to comprehensively assess monolayer adsorption capacity, surface heterogeneity, and adsorption energetics. Kinetic behavior was analyzed by applying the linear and nonlinear pseudo-first-order and pseudo-second-order models to describe the rate and mechanism of PFOS uptake. Using both fitting approaches provides a more robust evaluation of model suitability and improves the reliability of parameter estimation. All equilibrium and kinetic parameters were determined through regression analysis and used to interpret the dominant adsorption pathways governing PFOS removal.

2.9. Regeneration experiments

Regeneration experiments were conducted to assess the reusability and stability of the synthesized activated carbon. At the end of each adsorption cycle, the spent adsorbent was recovered and subsequently washed with an ethanol solution acidified to 0.1 mol L^{-1} of HCl to facilitate desorption of PFOS. The washed material was separated and then reintroduced into a fresh PFOS solution under the same operating conditions as the initial adsorption run. This adsorption–desorption procedure was repeated for five consecutive cycles, and the PFOS removal efficiency after each cycle was recorded to evaluate the adsorbent's regeneration performance and its stability during repeated reuse.

3. Results and discussion

3.1. Optimization of adsorbent synthesis

3.1.1. Analysis of variance and model adequacy

A Central Composite Design (CCD) was employed to optimize the synthesis conditions of the activated carbon with respect to its PFOS adsorption capacity (q_e). The experimental design considered impregnation ratio (A, IR), microwave power (B), and activation time (C) as independent variables, while the equilibrium adsorption capacity (q_e, mg g^{-1}) was selected as the response. The experimental matrix and corresponding q_e values are presented in Table S1. A quadratic polynomial model was fitted to describe the relationship between the synthesis parameters and q_e, as expressed in Eq. (2).

$$q_e = +12.25 + 5.22\,A + 3.75\,B + 1.17\,C - 5.78\,AB - 2.07\,AC + 2.58\,BC + 1.69\,A^2 + 4.44\,B^2 + 3.46\,C^2 \quad (2)$$

The statistical significance and adequacy of the developed quadratic model were evaluated using analysis of variance (ANOVA), summarized in Table 1. The model was highly significant, with an F-value of 54.59 and a p-value lower than 0.0001, indicating that the selected synthesis parameters collectively exert a strong influence on PFOS adsorption capacity. All linear terms (A, B, C), interaction terms (AB, AC, BC), and quadratic terms (A^2, B^2, C^2) were statistically significant ($p < 0.05$), confirming the presence of strong

curvature and interaction effects in the design space. The high coefficient of determination ($R^2 = 0.9840$) indicates that 98.4% of the variability in q_e is explained by the model. The predicted R^2 value (0.8870) shows reasonable agreement with the adjusted R^2 (0.9660), confirming the model's predictive reliability. Furthermore, the lack-of-fit was not significant ($p = 0.0905$), indicating that the model adequately represents the experimental data.

3.1.2. Model diagnostics

Diagnostic plots were used to evaluate the model's validity. Fig. 1a shows the normal probability plot of residuals, which reveals that the residuals are approximately normally distributed, confirming that the error terms do not violate the assumption of normality. In Fig. 1b, the predicted vs. actual plot demonstrates that the predicted values closely align with the actual experimental data, confirming the model's predictive strength. Lastly, Fig. 1c shows the residuals vs. predicted plot, which reveals that the model does not exhibit systematic bias, and there are no significant outliers in the residuals. These diagnostic results confirm that the quadratic model is statistically sound and suitable for navigating the synthesis design space to maximize PFOS adsorption capacity.

3.1.3. Effects of synthesis factors and their interactions

The perturbation plot (Fig. 2a) illustrates the relative influence of synthesis parameters on q_e while keeping other variables at their center levels. The impregnation ratio (A) exhibits the strongest effect on q_e, with adsorption capacity increasing markedly as IR increases within the studied range. This behavior indicates that higher phosphoric acid impregnation promotes pore development and surface functionalization, enhancing PFOS uptake.

Microwave power (B) shows a pronounced nonlinear effect on q_e. Moderate power levels lead to maximum adsorption capacity, whereas both insufficient and excessive power reduce q_e. At low power, incomplete activation limits pore formation, while excessive power likely causes partial pore collapse and structural degradation. Activation time (C) has a comparatively weaker but still significant effect, with q_e increasing at intermediate activation durations before declining at extended times due to over-activation and carbon burn-off.

The interaction between impregnation ratio and microwave power (Fig. 2b) reveals that high q_e values are achieved at high IR combined with moderate microwave power. At excessively high power levels, the positive effect of IR diminishes, indicating that aggressive heating overrides the benefits of chemical impregnation. Fig. 2c shows the interaction between impregnation ratio and activation time. At high IR values, q_e reaches a maximum at intermediate activation times, while prolonged activation results in reduced capacity due to excessive etching and loss of accessible pore volume.

The interaction between microwave power and activation time (Fig. 2d) further confirms the importance of controlled activation. Maximum q_e occurs at moderate power and intermediate time, whereas the combination of high power and long activation time leads to a pronounced decline in adsorption capacity, consistent with structural collapse of the carbon framework.

Overall, these response surface analyses demonstrate that q_e is governed primarily by the impregnation ratio, with microwave power exerting a strong nonlinear influence and activation time acting as a secondary tuning parameter. Optimal adsorption capacity is achieved only within a narrow synthesis window where pore development, surface functionality, and structural stability are simultaneously preserved.

3.1.4. Verification of optimal synthesis conditions

Numerical optimization was carried out to maximize PFOS adsorption capacity (q_e) based on the developed quadratic model. The optimal synthesis conditions were identified as an impregnation ratio of 3.0, microwave power of 500 W, and activation time of 10 min, under which the model predicted a maximum q_e value of 32.58 mg g^{-1} . A confirmation experiment performed at the optimized synthesis conditions yielded a q_e value within the model-predicted interval of 27.78–37.38 mg g^{-1} . The predicted mean q_e (32.58 mg g^{-1}) also lay within the 95% confidence interval (29.54–35.62 mg g^{-1}), confirming the reliability of the quadratic model and the robustness of the optimized synthesis conditions at a 95% confidence level.

Table 1
ANOVA results for the quadratic model during activated carbon synthesis optimization.

Source	Sum of Squares	df	Mean Square	F-value	p-value	
Model	1273.11	9	141.46	54.59	< 0.0001	significant
A-IR	371.84	1	371.84	143.49	< 0.0001	
B-Power	192.23	1	192.23	74.18	< 0.0001	
C-Time	18.59	1	18.59	7.17	0.0280	
AB	267.23	1	267.23	103.13	< 0.0001	
AC	34.26	1	34.26	13.22	0.0066	
BC	53.38	1	53.38	20.60	0.0019	
A^2	36.13	1	36.13	13.94	0.0058	
B^2	249.33	1	249.33	96.22	< 0.0001	
C^2	151.62	1	151.62	58.51	< 0.0001	
Residual	20.73	8	2.59			
Lack of Fit	18.77	5	3.75	5.75	0.0905	not significant
Pure Error	1.96	3	0.6534			
Cor Total	1293.85	17				

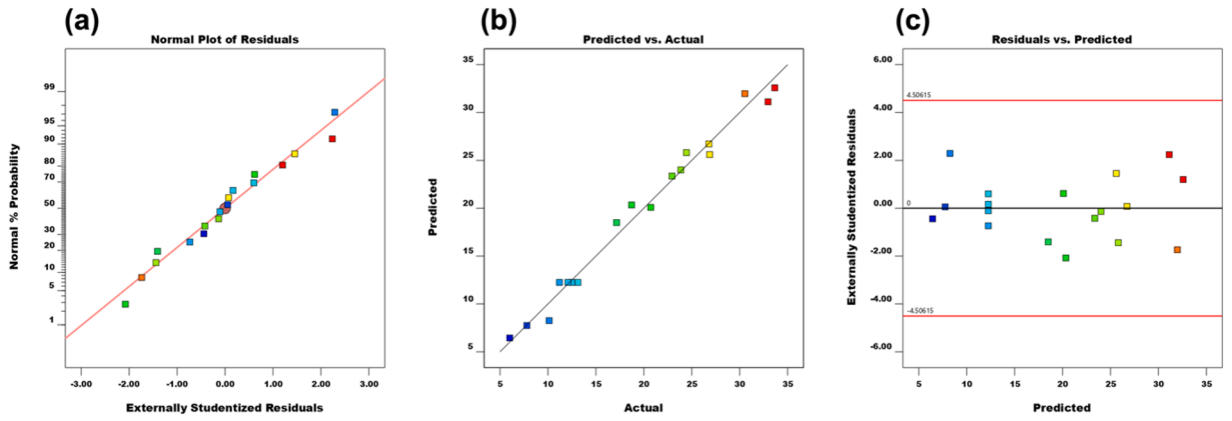

Fig. 1. Diagnostic plots for the synthesis optimization model; (a) normal probability plot of residuals; (b) predicted versus actual q_e values; (c) residuals versus predicted q_e.

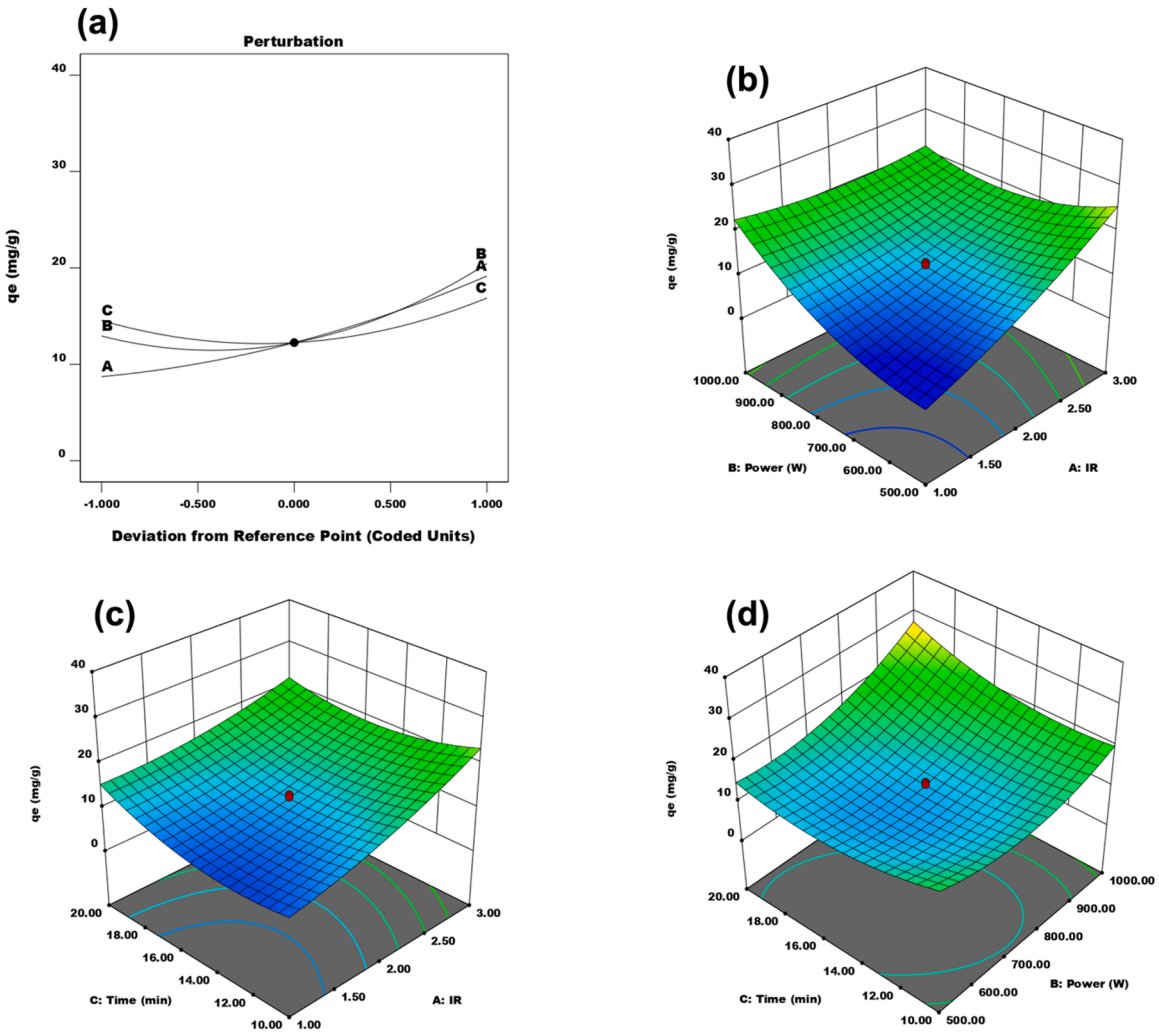

Fig. 2. Response surface plots for synthesis optimization showing the effects of synthesis parameters on PFOS adsorption capacity (q_e): (a) perturbation plot; (b) IR–power interaction; (c) IR–time interaction; (d) power–time interaction.

3.2. Characterization of the synthesized activated carbon

Proximate analysis of the raw compressed wood (Table S2) showed 7.7 % moisture, 1.3 % ash, 90.8 % volatile matter, and 0.2 % fixed carbon. The low ash content is advantageous for activated carbon production because excessive inorganic residues can inhibit pore development during activation. This composition is consistent with the porous morphologies observed in the structural analyses. BET measurements (Table S3) demonstrated a substantial increase in surface area and pore accessibility after phosphoric acid impregnation and microwave activation. The raw precursor exhibited a low surface area of 2.39 $m^2\ g^{-1}$ with an average pore diameter of 48.6 Å. After activation, the optimized adsorbent achieved a surface area of 1226 $m^2\ g^{-1}$ with a mesopore diameter near 24 Å, confirming the formation of a well-developed mesoporous structure. Among the tested samples, the highest-performing adsorbent displayed a surface area of 1030 $m^2\ g^{-1}$, whereas the least efficient sample showed 648 $m^2\ g^{-1}$, indicating that both impregnation ratio and microwave conditions influenced pore generation.

FESEM images at multiple magnifications (Fig. 3) reveal multiscale morphological features produced by phosphoric acid activation and microwave treatment. At the nanoscale (Fig. 3a), spherical carbon clusters and nano-sized pore entrances are visible, indicating the development of micro and mesopore openings. The images at 2 μm and 10 μm (Fig. 3b–c) show surface cracking and pore openings, while intermediate magnifications (Fig. 3d–e) reveal extensive fissures and interconnected channels. The large-scale image (Fig. 3f) displays fragmented macrostructures resulting from devolatilization and structural collapse. The observed multiscale morphological features indicate a hierarchical pore texture that is fundamentally conducive to PFOS transport. The presence of macro-scale fissures and surface cracking serves as low-resistance conduits for the rapid diffusion of PFOS molecules from the bulk solution to the internal framework. Once within the matrix, the well-developed mesopores (24.30 Å) provide the high specific surface area (1226 $m^2\ g^{-1}$) necessary for high-capacity monolayer adsorption. This structural hierarchy directly correlates with the high removal efficiency observed, as it minimizes mass-transfer limitations during the adsorption process.

The surface chemistry of the synthesized activated carbon before and after PFOS uptake was elucidated via FTIR spectroscopy (Fig. 4a). In the fresh adsorbent, a prominent O–H stretching band at 3422 cm^{-1} indicates an abundance of surface hydroxyl groups (Hsiao et al., 2025). The distinct feature at 1118 cm^{-1} is attributed to P–O–C/P–O stretching vibrations, confirming the successful incorporation of phosphate species during the microwave-assisted H_3PO_4 activation. Aromatic C═C stretching at 1561 cm^{-1} signifies the stable lignin-derived framework of the wood precursor. Upon PFOS adsorption, significant modifications are observed in the spectra. The O–H band at 3422 cm^{-1} exhibits noticeable broadening and a shift in intensity, while the phosphate-associated band at

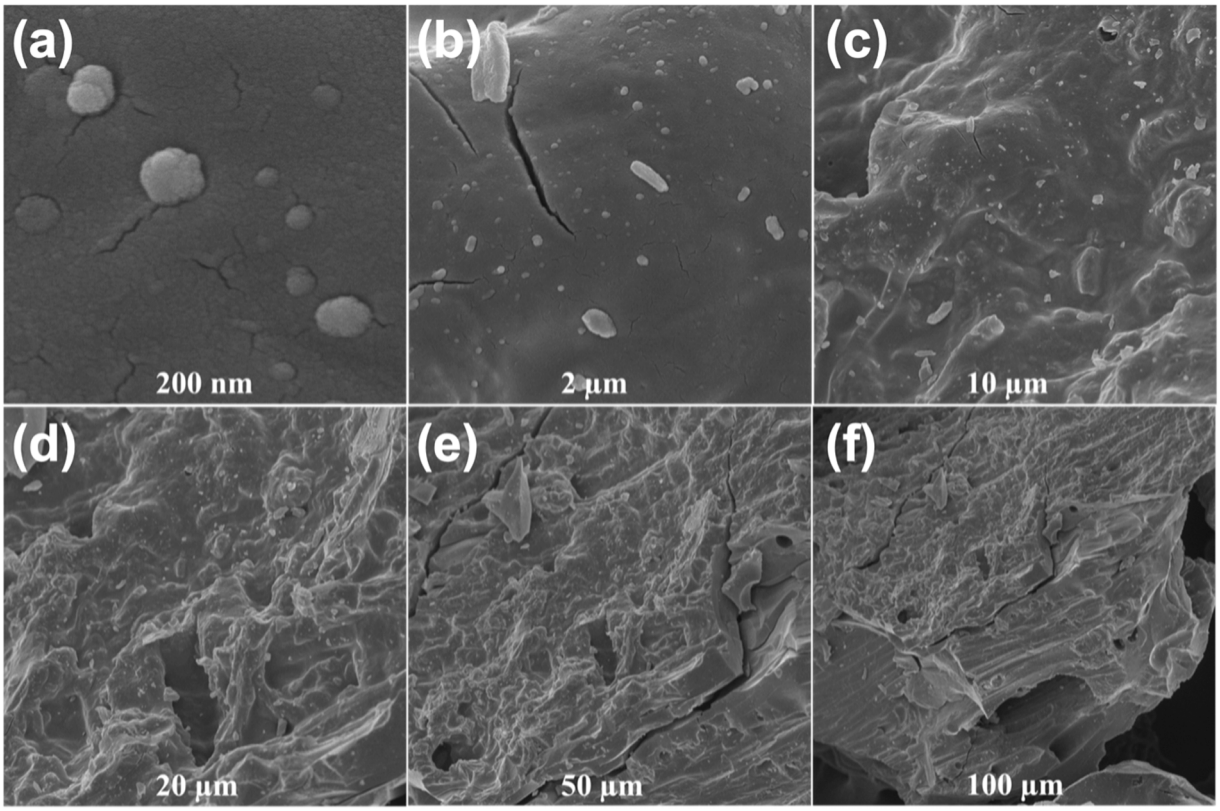

Fig. 3. FESEM images of the synthesized activated carbon at different magnifications; (a) 200 nm; (b) 2 μm; (c) 10 μm; (d) 20 μm; (e) 50 μm; (f) 100 μm.

1118 cm^{-1} shows a clear reduction in transmittance. These alterations provide direct evidence that the surface hydroxyl and phosphate functionalities serve as primary active sites, facilitating hydrogen bonding and electrostatic attraction with the anionic sulfonate headgroup of the PFOS molecule. Meanwhile, the relative stability of the aromatic C═C peaks suggests that the graphitic domains remain available for hydrophobic interactions with the perfluorinated tail of the adsorbate.

The Raman spectrum (Fig. 4b) displays characteristic D and G bands at 1356 cm^{-1} and 1649 cm^{-1} , respectively. The Raman I_D/I_G ratio of 0.66 signifies a balanced structural configuration, where the presence of graphitic sp^2 domains facilitates hydrophobic interactions with the fluorinated tail of PFOS, while the defect-rich regions provide accessible active sites for chemical bonding. This moderate degree of disorder is critical for ensuring that both physical and chemical adsorption pathways are simultaneously active.

EDS analysis (Fig. S1) revealed that the activated carbon is predominantly composed of carbon (88.67%), with oxygen (7.59%) and phosphorus (3.74%) incorporated into its structure. This composition aligns with the oxygenated functionalities observed in FTIR and the phosphorus introduced during H_3PO_4 activation. Elemental mapping further confirmed the uniform distribution of these heteroatoms across the matrix.

Overall, the combined results from BET surface analysis, FESEM morphology, FTIR functional group identification, Raman structural assessment, and EDS elemental mapping demonstrate that the synthesized activated carbon possesses a hierarchical pore structure, diverse surface functionalities, and heteroatom incorporation that collectively create a favorable environment for PFOS adsorption.

3.3. Optimization of PFOS removal efficiency

3.3.1. Model development and statistical analysis

Response surface methodology (RSM) was employed to evaluate and optimize the combined effects of contact time (A), adsorbent dosage (B), solution pH (C), and initial PFOS concentration (D) on PFOS removal efficiency (%). A central composite design consisting of 29 experimental runs was used, and the corresponding experimental and model-predicted removal efficiencies are summarized in Table S4. A second-order polynomial model was fitted to the data to describe the response as a function of the operational variables, as expressed in Eq. (3).

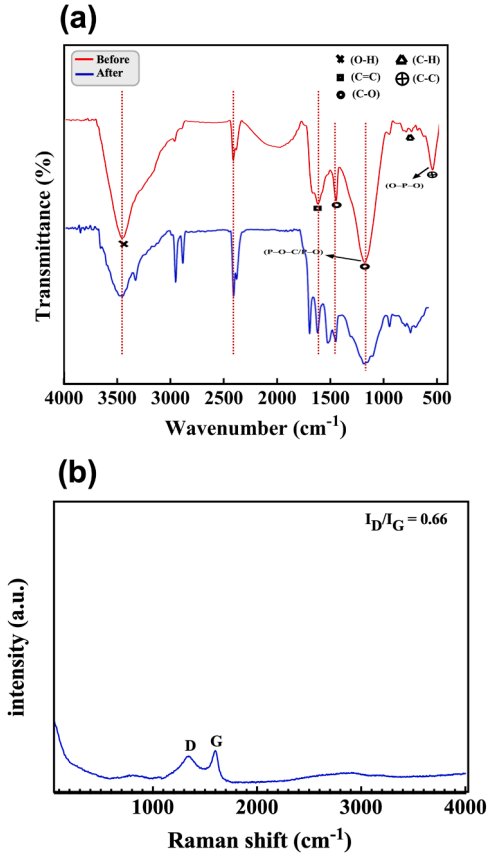

Fig. 4. (a) FTIR spectrum before and after adsorption; (b) Raman spectrum of the synthesized activated carbon.

$$\begin{aligned} \textit{PFOS removal}\ (\%) = {} & 118.83 + 8.22\ A - 13.40\ B - 17.49\ C - 1.19\ D + 0.82\ AB - 0.36\ AC \\ & + 0.07\ AD + 4.40\ BC - 0.36\ BD - 0.08\ CD - 0.60\ A^2 + 3.07\ B^2 + 0.92\ C^2 + 0.02\ D^2 \end{aligned} \quad (3)$$

Analysis of variance (ANOVA) results for the quadratic model are presented in Table 2. The model exhibited a high F-value of 55.28 with a p-value < 0.0001, confirming that the regression is statistically significant and that the selected operational variables collectively exert a strong influence on PFOS removal. The coefficient of determination ($R^2 = 0.9835$) indicates that more than 98% of the variability in removal efficiency is explained by the model. The adjusted R^2 (0.9657) and predicted R^2 (0.9026) show good agreement, confirming the model's predictive reliability and absence of overfitting. The Adeq Precision value of 27.05, well above the minimum desirable value of 4, demonstrates a strong signal-to-noise ratio and confirms that the model can be reliably used to navigate the design space.

Among the main effects, contact time, adsorbent dosage, solution pH, and initial PFOS concentration were all highly significant ($p < 0.0001$). Significant interaction effects were observed between adsorbent dosage and pH (BC), adsorbent dosage and initial PFOS concentration (BD), and pH and initial PFOS concentration (CD), indicating that PFOS removal efficiency is governed by coupled interactive mechanisms rather than independent factor effects. The quadratic terms for pH (C^2) and initial PFOS concentration (D^2) were also significant, confirming the presence of curvature in the response surface and the existence of an optimal operational window. The lack-of-fit was not significant ($p = 0.0798$), indicating that the quadratic model adequately represents the experimental data within the studied ranges.

3.3.2. Model diagnostics and validation

Model adequacy was further verified using diagnostic plots (Fig. S2). The normal probability plot of externally studentized residuals (Fig. S2a) shows an approximately linear distribution, confirming that the residuals follow a normal distribution. The predicted versus experimental removal efficiency plot (Fig. S2b) exhibits close clustering of data points along the 1:1 line, demonstrating excellent agreement between model predictions and experimental observations.

The residuals versus predicted values plot (Fig. S2c) reveals a random scatter without discernible trends, indicating homoscedasticity and the absence of systematic model bias. Although a limited number of data points exceeded the studentized residual threshold, Cook's distance analysis confirms that these points do not exert disproportionate influence on the fitted model. Collectively, these diagnostics confirm that the developed quadratic model is statistically robust and suitable for interpreting the effects of operational parameters on PFOS removal efficiency.

3.3.3. Effects of operational parameters on PFOS removal efficiency

The perturbation plot (Fig. S2d) illustrates the relative influence of each operational variable on PFOS removal efficiency while holding other factors at their center levels. Initial PFOS concentration (D) and solution pH (C) exerted the strongest effects on removal efficiency, followed by adsorbent dosage (B) and contact time (A).

Removal efficiency increased markedly with increasing contact time, reflecting progressive diffusion of PFOS molecules into the mesoporous structure and gradual occupation of accessible adsorption sites. Adsorbent dosage exhibited a strong positive effect on removal efficiency, as higher dosages provide a larger number of active sites relative to PFOS mass in solution. In contrast to qe-based optimization, this trend directly reflects practical treatment performance rather than mass-normalized site utilization.

Solution pH showed a pronounced negative effect on PFOS removal efficiency, with acidic conditions favoring adsorption. This behavior is attributed to enhanced electrostatic attraction between protonated oxygen-containing surface functional groups and the

Table 2
ANOVA results for the quadratic model of PFOS removal efficiency optimization.

Source	Sum of Squares	df	Mean Square	F-value	p-value	
Model	11757.05	14	839.79	55.28	< 0.0001	significant
A-Time	1777.79	1	1777.79	117.03	< 0.0001	
B-Adsorbent	1645.47	1	1645.47	108.32	< 0.0001	
C-pH	2011.65	1	2011.65	132.42	< 0.0001	
D-Initial PFOS	2992.21	1	2992.21	196.97	< 0.0001	
AB	11.16	1	11.16	0.7343	0.4070	
AC	33.18	1	33.18	2.18	0.1633	
AD	53.29	1	53.29	3.51	0.0837	
BC	481.62	1	481.62	31.70	< 0.0001	
BD	217.42	1	217.42	14.31	0.0023	
CD	183.60	1	183.60	12.09	0.0041	
A^2	59.15	1	59.15	3.89	0.0701	
B^2	36.25	1	36.25	2.39	0.1464	
C^2	744.44	1	744.44	49.00	< 0.0001	
D^2	846.35	1	846.35	55.71	< 0.0001	
Residual	197.49	13	15.19			
Lack of Fit	179.84	9	19.98	4.53	0.0798	not significant
Pure Error	17.64	4	4.41			
Cor Total	11954.54	27				

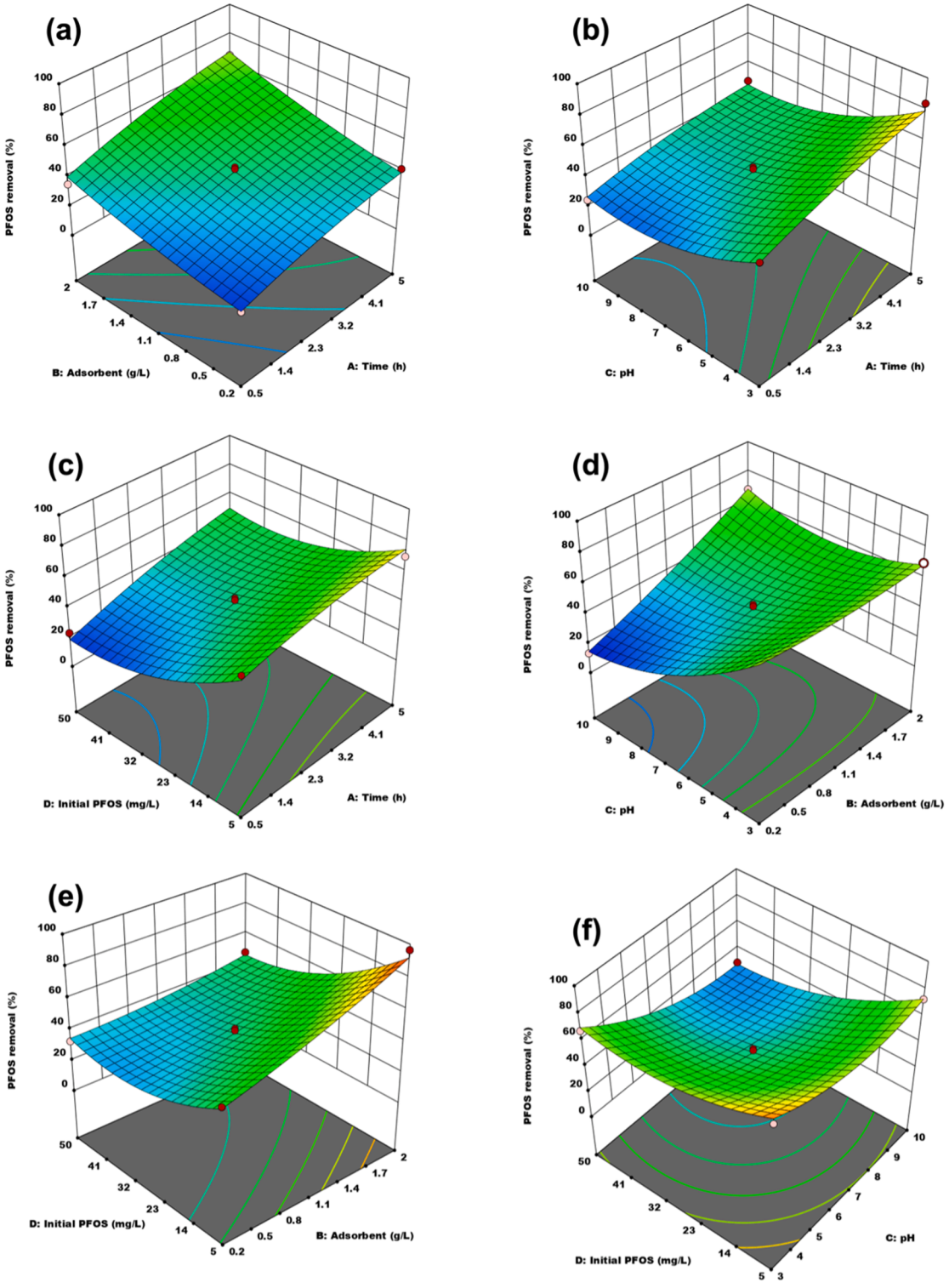

Fig. 5. Three-dimensional response surface plots showing the interactive effects of operational parameters on PFOS removal efficiency: (a) contact time–adsorbent dosage; (b) contact time–pH; (c) contact time–initial PFOS concentration; (d) adsorbent dosage–pH; (e) adsorbent dosage–initial PFOS concentration; (f) pH–initial PFOS concentration.

anionic sulfonate headgroup of PFOS. Initial PFOS concentration displayed a nonlinear effect, removal efficiency decreased at higher concentrations due to site saturation, despite the higher mass-transfer driving force.

3.3.4. Interaction effects and response surface analysis

Three-dimensional response surface plots illustrating the interactive effects of operational variables on PFOS removal efficiency are presented in Fig. 5. The interaction between contact time and adsorbent dosage (Fig. 5a) indicates that near-complete PFOS removal can be achieved at longer contact times combined with higher dosages, confirming that sufficient residence time and site availability are critical for maximizing treatment efficiency.

The interaction between contact time and pH (Fig. 5b) shows that acidic conditions consistently enhance removal efficiency across all contact times, whereas alkaline conditions limit PFOS uptake even with prolonged contact. This result underscores the dominant role of surface charge interactions in PFOS adsorption. The interaction between contact time and initial PFOS concentration (Fig. 5c) reveals that removal efficiency decreases at higher PFOS concentrations, particularly at shorter contact times, likely because the system has not reached equilibrium, and adsorption sites are not fully utilized. Increasing contact time allows the system to stabilize, promoting deeper intraparticle diffusion and improving removal efficiency.

The response surface describing adsorbent dosage and pH (Fig. 5d) demonstrates that pH effects are more pronounced at lower dosages, where adsorption is governed by surface chemistry rather than site abundance. The interaction between adsorbent dosage and initial PFOS concentration (Fig. 5e) confirms that higher dosages are required to maintain high removal efficiency at elevated PFOS concentrations. Finally, the interaction between pH and initial PFOS concentration (Fig. 5f) shows that acidic conditions mitigate the negative impact of higher PFOS concentrations by strengthening electrostatic attraction. Collectively, these response surfaces confirm that PFOS removal efficiency is governed by coupled effects of surface chemistry, site availability, and mass-transfer limitations, emphasizing the necessity of multivariable optimization.

3.3.5. Optimum conditions and confirmation

Numerical optimization was performed to maximize PFOS removal efficiency within the studied operational ranges. At an initial PFOS concentration of 5 mg L^{-1} , the optimal conditions were identified as a contact time of 4.82 h, adsorbent dosage of 1.95 g L^{-1} ,

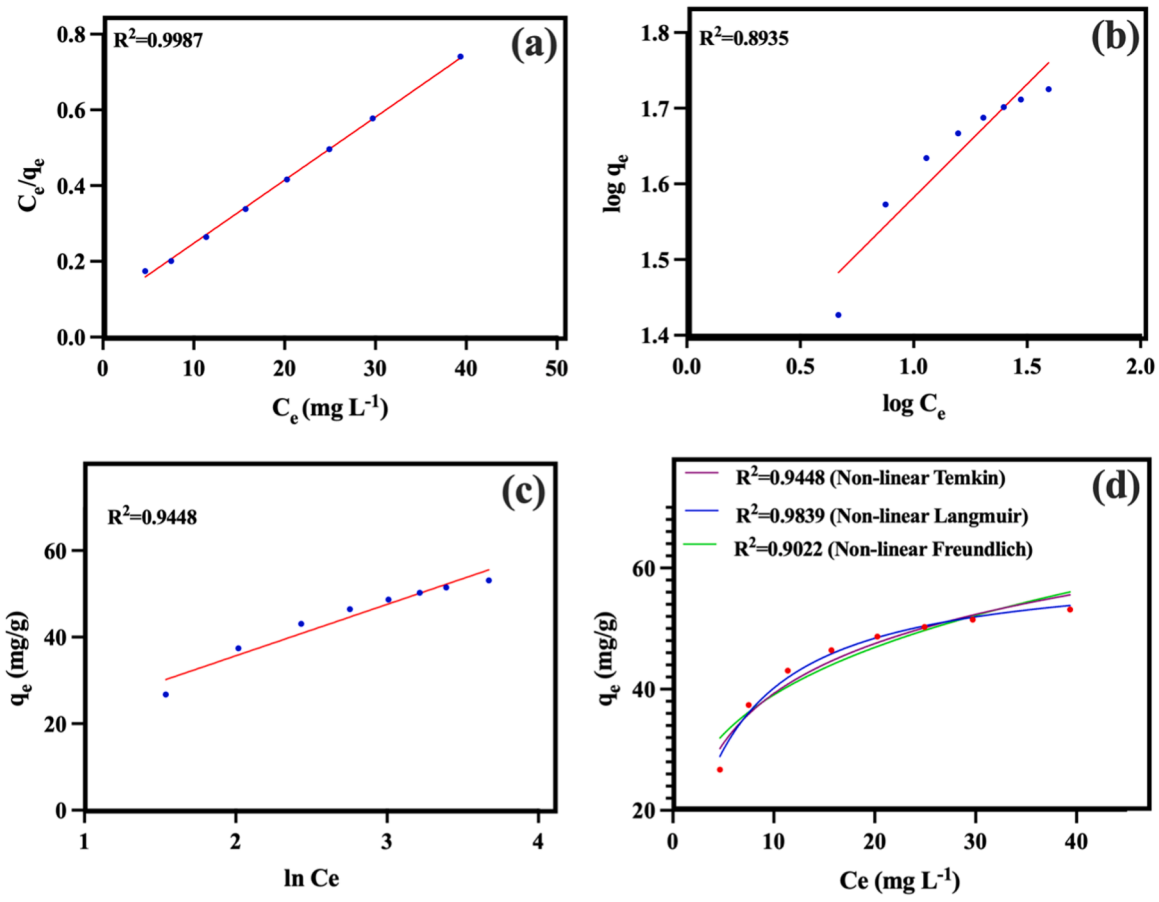

Fig. 6. Linear and non-linear adsorption isotherm models for PFOS adsorption on the adsorbent: (a) linear Langmuir, (b) Freundlich, (c) Temkin and (d) nonlinear models.

and solution pH of 7.0, yielding a predicted removal efficiency of 97.87% with a desirability of 1.00. Notably, the optimization was performed under natural pH conditions (pH of 7.0), which enhances the practicality and cost-effectiveness of the process for real-world water treatment applications.

The confirmation experiment conducted under these optimized conditions produced an experimental removal efficiency of 96.23%, which lies within the model's 95% prediction interval (PI) of 78.39–114.63%. This confirms the reliability of the regression model and validates the robustness of the optimized operational conditions for effective PFOS removal.

3.4. Adsorption mechanism

3.4.1. Adsorption isotherm study

The adsorption of PFOS onto the synthesized activated carbon was assessed to understand the equilibrium distribution of PFOS between the water phase and the adsorbent surface. The isotherm plots are presented in Fig. 6, and the fitted parameters for both linear and non-linear models are provided in Table S5. As the equilibrium PFOS concentration increased, the removal efficiency showed a small decrease, while the adsorption capacity (q_e) gradually increased.This trend indicates a stronger mass-transfer driving force at higher concentrations and suggests the sequential occupation of higher-energy adsorption sites followed by progressively weaker sites, which is characteristic of surface-limited adsorption on a heterogeneous carbon matrix.

The high adsorption capacity observed across the equilibrium range aligns well with the structural and chemical attributes of the activated carbon. BET analysis verified the development of a high-surface-area mesoporous structure (up to 1226 $m^2\ g^{-1}$, mesopore diameter approximately 24 Å), supplying abundant accessible sites for PFOS transport. FESEM images suggested the presence of multi-scale pore openings that are consistent with a hierarchical pore environment and promote intraparticle diffusion. FTIR spectra confirmed the presence of oxygen-containing surface groups, while Raman analysis ($I_D/I_G = 0.66$) indicated a combination of graphitic domains and defect-rich regions. These features collectively support multiple interaction pathways for PFOS, including hydrophobic interactions with the carbon matrix, electrostatic attraction between protonated oxygenated groups and the PFOS sulfonate head-group, and π–π interactions with aromatic carbon domains.

The equilibrium data were analyzed using the Langmuir, Freundlich, and Temkin isotherm models in both linear and non-linear forms (Fig. 6). Among these, the non-linear Langmuir model showed the best fit to the experimental results ($R^2 = 0.9839$), suggesting that PFOS adsorption mainly occurs as a monolayer on uniform surface sites. The Langmuir parameters ($q_{max} = 60.85\ mg\ g^{-1}$ and $K_L = 0.194\ L\ mg^{-1}$) indicate a strong interaction between PFOS molecules and the active sites of the adsorbent. This monolayer adsorption behavior is consistent with the mesoporous structure revealed by BET analysis, where a high number of accessible sites allows even occupation of the surface.

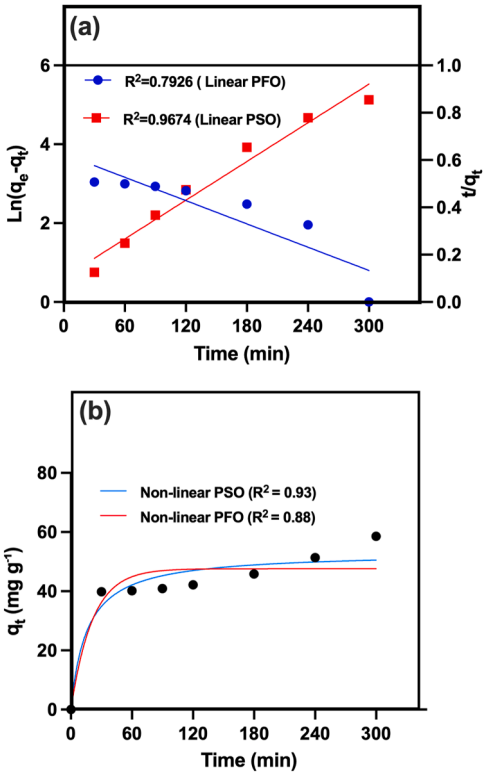

Fig. 7. Linear and non-linear fits of PFO and PSO kinetic models for PFOS adsorption.

The Freundlich model also provided a relatively strong correlation ($R^2 = 0.9022$), with parameters $K_f = 21.30$ and $n = 3.79$, indicating highly favorable adsorption (n greater than 1) and moderate surface heterogeneity. This heterogeneity is consistent with the diverse functional environments suggested by FTIR and Raman spectroscopy, confirming the coexistence of graphitic domains and defect-rich regions. These varied sites contribute simultaneously to electrostatic interactions, hydrophobic interactions, and π-interactions during PFOS uptake.

The Temkin isotherm ($A = 2.73$ and $B = 11.89$ J mol^{-1}, $R^2 = 0.9448$) also described the data well, suggesting that the heat of adsorption decreases gradually with increasing surface coverage. This behavior is expected for PFOS adsorption on a functionalized carbon surface, where adsorption initially occurs at higher-energy sites and is followed by weaker interactions at defect-modified or heteroatom-containing regions.

Taken together, the isotherm results confirm that PFOS adsorption onto the synthesized activated carbon is dominated by a Langmuir-type monolayer mechanism, with complementary evidence of surface heterogeneity consistent with the Freundlich and Temkin models. The combined structural features of the adsorbent, including high surface area, accessible mesoporosity, and chemically diverse surface sites, enable efficient PFOS uptake through multiple simultaneous adsorption pathways.

Based on the combined characterization and adsorption results, PFOS removal by the synthesized activated carbon is proposed to occur through a synergistic multimodal mechanism. The mesoporous structure and high specific surface area facilitate rapid diffusion and pore-filling of PFOS molecules within the carbon matrix. Simultaneously, graphitic carbon domains promote hydrophobic interactions with the fluorinated PFOS tail, while oxygen- and phosphorus-containing surface functionalities contribute to electrostatic attraction and hydrogen-bond-assisted interactions with the sulfonate headgroup. The coexistence of these mechanisms likely explains the high adsorption efficiency achieved under neutral pH conditions, where purely electrostatic adsorption would normally be less favorable.

3.4.2. Kinetics

The adsorption kinetics of PFOS on the synthesized activated carbon were studied using pseudo-first-order (PFO) and pseudo-second-order (PSO) models in both linear and non-linear forms to clarify the adsorption rate and the controlling mechanism. The experimental kinetic data and the corresponding model fits are shown in Fig. 7.

The linear PFO model showed limited agreement with the experimental data, as evidenced by noticeable deviations at longer contact times. Although the PFO model describes the initial uptake reasonably well, its inability to accurately capture the full adsorption process suggests that PFOS removal cannot be represented solely by a first-order mass-transfer mechanism.

In contrast, the PSO model provided a substantially improved description of the kinetic behavior. Both linear and non-linear PSO fittings showed higher correlation with the experimental data compared to the PFO model, indicating that the adsorption process is predominantly governed by surface-controlled interactions rather than external diffusion alone. The superior performance of the non-linear PSO model, in particular, reflects its ability to accurately describe the entire adsorption period, from rapid initial uptake to gradual approach toward equilibrium.

It should be noted that equilibrium adsorption capacities obtained from kinetic model fitting are model-dependent parameters and do not necessarily represent the true adsorption capacity of the adsorbent. Therefore, kinetic-derived capacity values were not interpreted as maximum adsorption capacities. Instead, adsorption capacity was evaluated based on equilibrium isotherm analysis, which provides a more reliable representation of monolayer adsorption behavior (Lima et al., 2021).

The dominance of pseudo-second-order kinetics suggests that PFOS adsorption is controlled by interactions between the adsorbate and active sites on the carbon surface. This behavior is consistent with the physicochemical characteristics of the synthesized activated carbon, including its high surface area, well-developed mesoporous structure, and the presence of oxygen- and phosphorus-containing surface functional groups. These features promote strong surface interactions with the PFOS sulfonate headgroup, facilitating rapid

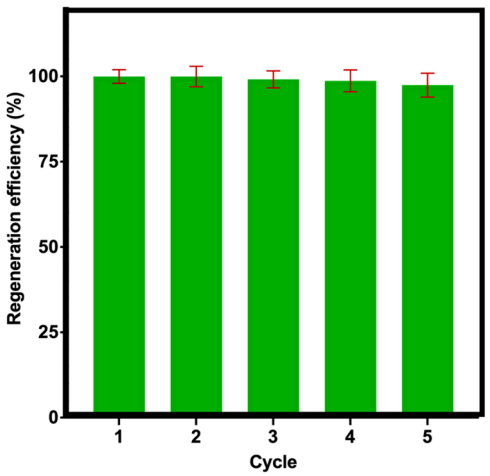

Fig. 8. Regeneration performance of the adsorbent over adsorption–desorption cycles.

adsorption followed by progressive site occupation (Shin and An, 2024; Zhang, 2019).

Overall, the kinetic analysis confirms that PFOS adsorption onto the synthesized activated carbon follows pseudo-second-order behavior, indicating that surface-mediated interactions play a central role in controlling the adsorption rate.

3.5. Regeneration performance

Ensuring that an adsorbent maintains its performance over multiple cycles is essential for its practical application in PFOS treatment. To evaluate the durability of the synthesized activated carbon, five consecutive adsorption–desorption cycles were conducted using an ethanol solution acidified with 0.1 mol L^{-1} HCl as the regenerating medium. Regeneration efficiency in this study refers to how closely the removal performance in each cycle approaches the initial adsorption capacity. The activated carbon demonstrated excellent reusability, retaining more than 95 % of its initial PFOS removal efficiency after five cycles (Fig. 8). This high level of stability indicates that the structural and chemical attributes of the material remain largely preserved during repeated adsorption and desorption events.

The strong regeneration behavior can be understood in part from the structural and chemical characteristics of the fresh adsorbent. BET analysis indicated a high-surface-area mesoporous structure that provides accessible pathways for both PFOS transport and penetration of the regenerating solution. FESEM images also showed open pore channels that enable diffusion into internal regions of the adsorbent. In addition, FTIR spectra of the fresh material confirmed the presence of oxygen-containing functionalities such as hydroxyl and C–O groups. These groups can be protonated under acidic conditions, which weakens their interaction with the PFOS sulfonate headgroup and facilitates desorption.

The superior regeneration efficiency observed with HCl-modified ethanol is attributed to its ability to weaken PFOS–surface interactions by lowering the pollutant's charge density. The acidic environment reduces the electrostatic attraction between the PFOS sulfonate group and the oxygen-containing surface functionalities, while ethanol improves solvation of the partially protonated PFOS molecules. This combined effect promotes efficient desorption of PFOS from within both the external pore surfaces and the deeper mesoporous regions (Ranjbar et al., 2024).

Overall, the regeneration results demonstrate that the synthesized activated carbon possesses a highly stable structure and surface chemistry, enabling repeated use with minimal loss in efficiency. This excellent reusability, combined with its low-cost biomass origin and strong PFOS affinity, highlights the material's suitability for sustainable water treatment systems and long-term operational applications.

3.6. Comparison with literature

The performance of the activated carbon synthesized in this study was evaluated in the context of representative PFOS adsorbents reported in the literature, with emphasis on removal efficiency and pH dependence. A concise comparison is presented in Table 3.

As shown in the table, a wide range of advanced adsorbents, including metal–organic frameworks (MOFs), porous organic polymers (POPs), modified biochars, and hybrid composites, have been reported to achieve high PFOS removal efficiencies. However, the majority of these materials exhibit optimal performance under acidic conditions, typically in the pH range of 2.5–5. Adsorbents such as MOF−808, DUT−5–2, MIL−53-based frameworks, POP−3, POP−7, graphite intercalated compounds, and chitosan- or hydrogel-based composites rely predominantly on electrostatic attraction between positively charged surface sites and the anionic sulfonate group of PFOS. As solution pH increases toward neutral values, surface deprotonation and increased competition from co-existing anions reduce adsorption efficiency, limiting their applicability in real water matrices.

In contrast, the activated carbon developed in this work achieved a high PFOS removal efficiency of approximately 97.9 % at natural pH (pH $\approx$ 7), without the need for chemical pH adjustment. This behavior distinguishes the present adsorbent from most reported PFOS adsorbents and represents a key practical advantage. Recent studies on PFOS adsorption have increasingly focused on highly engineered porous materials with strong adsorption capacities but limited operational practicality due to pH sensitivity, synthesis complexity, or regeneration challenges. In contrast, the present work emphasizes simultaneous adsorption efficiency, operational simplicity, and scalability under environmentally relevant conditions.

pH adjustment increases chemical consumption, operational complexity, and cost, and is often impractical in full-scale water and wastewater treatment systems. The ability of the present adsorbent to operate effectively under environmentally relevant pH

Table 3
Comparison of PFOS removal efficiency and optimal pH of reported adsorbents.

Adsorbent	PFOS removal (%)	Optimal pH	Reference
This study	97.9	7 (natural)	-
Commercial activated carbon	93	5–7	(Pala et al., 2023)
MOF−808	High	4–5	(Chang et al., 2022)
DUT−5–2	96.6	3	(Hu et al., 2022)
POP−3	97.8	4	(Elboughdiri et al., 2023)
Acid-modified biochar	High	2–5	(Zhang et al., 2023)
Hybrid hydrogel	91.6	3	(Zakaria et al., 2023)
Graphite intercalated compound	> 95	3	(Trzcinski and Harada, 2024)
Layered double hydroxide (LDH)	High	2.5	(Chen et al., 2021)

conditions therefore enhances its potential for real-world application.

Commercial activated carbons typically show PFOS removal efficiencies around 90–93 % over a moderately broad pH range (approximately pH 5–7). The activated carbon synthesized in this study provides higher removal efficiency while being produced from a discarded compressed wood precursor through a rapid microwave-assisted activation process. Compared with conventional furnace-based activation methods that require prolonged heating and high energy input, microwave activation enables fast and energy-efficient synthesis, improving the sustainability and scalability of the material.

Beyond pH performance, the adsorption behavior of the present activated carbon differs mechanistically from many acidic-pH-optimized materials. The well-developed mesoporous structure promotes efficient intraparticle diffusion, while oxygen-containing surface functionalities and graphitic domains support PFOS uptake through a combination of pore filling, hydrophobic interactions, and electrostatic attraction. This multimodal adsorption mechanism contributes to reduced pH sensitivity and stable performance under neutral conditions. In addition, the adsorbent exhibited excellent reusability, maintaining more than 95 % of its initial PFOS removal efficiency over multiple adsorption–desorption cycles, further supporting its suitability for practical application.

In addition to removal efficiency, the present adsorbent also demonstrates advantages in synthesis simplicity and operational practicality compared with several previously reported PFOS adsorbents. Many high-performance materials such as MOFs and porous organic polymers require multi-step synthesis routes, expensive precursors, or strict operating conditions, which may limit large-scale implementation. In contrast, the activated carbon developed in this work was synthesized from discarded compressed wood through a rapid microwave-assisted activation process using a low-cost precursor and short activation duration. Furthermore, the combination of high removal efficiency, operation at natural pH, and strong regeneration stability distinguishes the present material from many previously reported PFOS adsorbents that exhibit higher sensitivity to pH or reduced long-term reusability.

Overall, the comparison demonstrates that, while many advanced PFOS adsorbents achieve high removal efficiencies under acidic conditions, their strong pH dependence constrains large-scale implementation. The activated carbon developed in this study combines high PFOS removal efficiency at natural pH, a low-cost waste-derived precursor, energy-efficient microwave activation, and strong operational stability, positioning it as a practical and scalable alternative for PFOS treatment in real water and wastewater systems.

4. Conclusions

Activated carbon synthesized from discarded compressed wood through phosphoric acid impregnation and microwave assisted activation demonstrated strong potential for PFOS removal from aqueous systems. Optimization of the synthesis conditions produced an adsorbent with high surface area, well developed mesoporosity, and abundant oxygen and phosphorus containing surface functionalities, which collectively enhanced adsorption performance. Response surface methodology was successfully applied to optimize the adsorption process, identifying operating conditions of 4.82 h contact time, 1.95 g L^{-1} adsorbent dosage, and natural solution pH of 7.0, under which PFOS removal efficiencies exceeding 96 % were achieved at an initial concentration of 5 mg L^{-1} . The ability to attain high removal efficiency under neutral pH conditions represents a key practical advantage by eliminating the need for pH adjustment in real water treatment applications. Adsorption behavior followed the nonlinear Langmuir isotherm and pseudo second order kinetics, indicating monolayer adsorption governed by surface controlled interactions. The adsorbent also exhibited excellent regeneration performance, retaining more than 95 % of its removal efficiency after multiple reuse cycles. Overall, the combination of waste derived precursor utilization, energy efficient microwave assisted synthesis, high removal efficiency, and strong reusability highlights the suitability of this adsorbent for scalable PFOS remediation in water and wastewater treatment systems.

CRediT authorship contribution statement

Mahdi Maleki Lonbar: Writing – review & editing, Writing – original draft, Visualization, Software, Investigation, Conceptualization. **Mona Ardebilipour:** Writing – review & editing, Writing – original draft, Validation, Software, Investigation, Formal analysis, Conceptualization. **Majid Baghdadi:** Writing – original draft, Validation, Supervision, Project administration, Investigation, Funding acquisition, Formal analysis, Data curation, Conceptualization. **Ghufran Redzwan:** Writing – original draft, Validation, Investigation, Conceptualization.

Declaration of Competing Interest

The authors declare that they have no known competing financial interests or personal relationships that could have appeared to influence the work reported in this paper.

Acknowledgement

The authors wish to acknowledge the Nanotechnology Research Center of Graduate Faculty of Environment, University of Tehran, to support this research.

Appendix A. Supporting information

Supplementary data associated with this article can be found in the online version at doi:10.1016/j.eti.2026.105048.

Data availability

Data will be made available on request.

References

Abdelsamad, A.M.A., Saeidi, N., Mackenzie, K., 2025. Mesoporous silica nanoparticles for rapid removal of PFOA: impact of surface functional groups on adsorption efficiency and adsorbent regeneration. Environ. Pollut. 383. https://doi.org/10.1016/j.envpol.2025.126796.

Ao, W., Mian, M.M., Zhang, Q., Zhou, Z., Deng, S., 2024. Bamboo-derived low-cost mesoporous biochar for efficient removal of per- and polyfluoroalkyl substances from contaminated water. ACS ES T Water 4, 2711–2720. https://doi.org/10.1021/acsestwater.4c00211.

Bosch, D., Back, J.O., Gurtner, D., Giberti, S., Hofmann, A., Bockreis, A., 2022. Alternative feedstock for the production of activated carbon with ZnCl2: forestry residue biomass and waste wood. Carbon Resour. Convers. 5, 299–309. https://doi.org/10.1016/j.crcon.2022.09.001.

Boyer, T.H., Fang, Y., Ellis, A., Dietz, R., Choi, Y.J., Schaefer, C.E., Higgins, C.P., Strathmann, T.J., 2021. Anion exchange resin removal of per- and polyfluoroalkyl substances (PFAS) from impacted water: a critical review. Water Res. 200, 117244. https://doi.org/10.1016/j.watres.2021.117244.

Chang, P.-H., Chen, C.-Y., Mukhopadhyay, R., Chen, W., Tzou, Y.-M., Sarkar, B., 2022. Novel MOF-808 metal–organic framework as highly efficient adsorbent of perfluorooctane sulfonate in water. J. Colloid Interface Sci. 623, 627–636. https://doi.org/10.1016/j.jcis.2022.05.050.

Chen, Y., Georgi, A., Zhang, W., Kopinke, F.-D., Yan, J., Saeidi, N., Li, J., Gu, M., Chen, M., 2021. Mechanistic insights into fast adsorption of perfluoroalkyl substances on carbonate-layered double hydroxides. J. Hazard. Mater. 408. https://doi.org/10.1016/j.jhazmat.2020.124815.

Chen, Y., Zhu, J., Ma, H., Gu, Y., Liu, T., 2024. Fe2+-NTA synergized UV254 photolytic defluorination of perfluorooctane sulfonate (PFOS): enhancing through intramolecular electron density perturbation via electron acquisition. Water Res. 254. https://doi.org/10.1016/j.watres.2024.121421.

Cheng, J., Islam, M.T., Sadmani, A.H.M.A., Chang, N.-B., 2024. The effect of biochar in a specialty adsorbent on enhanced PFAS removal from surface water. J. Water Process. Eng. 67. https://doi.org/10.1016/j.jwpe.2024.106231.

Choudhary, A., Dong, D., Tsianou, M., Alexandridis, P., Bedrov, D., 2022. Adsorption mechanism of perfluorooctanoate on cyclodextrin-based polymers: probing the synergy of electrostatic and hydrophobic interactions with molecular dynamics simulations. ACS Mater. Lett. 4, 853–859. https://doi.org/10.1021/acsmaterialslett.2c00168.

Elboughdiri, N., Amari, A., Harharah, H.N., Al-Ansari, N., Sammen, S.S., 2023. Tailoring porous organic polymers with enhanced capacity, thermal stability and surface area for perfluorooctane sulfonic acid (PFOS) elimination from water environment. Appl. Water Sci. 13, 211.

Hassan, M., Du, J., Liu, Y., Naidu, R., Zhang, J., Ahsan, M.A., Qi, F., 2022. Magnetic biochar for removal of perfluorooctane sulphonate (PFOS): interfacial interaction and adsorption mechanism. Environ. Technol. Innov. 28. https://doi.org/10.1016/j.eti.2022.102593.

Hsiao, K.-Y., Chung, R.-J., Chang, P.-P., Tsai, T.-H., 2025. Identification of hydroxyl and polysiloxane compounds via infrared absorption spectroscopy with targeted noise analysis. Polymers 17, 1533. https://doi.org/10.3390/polym17111533.

Hu, Y., Guo, M., Zhang, S., Jiang, W., Xiu, T., Yang, S., Kang, M., Dongye, Z., Li, Z., Wang, L., 2022. Microwave synthesis of metal-organic frameworks absorbents (DUT-5-2) for the removal of PFOS and PFOA from aqueous solutions. Microporous Mesoporous Mater. 333, 111740. https://doi.org/10.1016/j.micromeso.2022.111740.

Huang, X., Huang, J., Wang, K., Hao, M., Geng, M., Shi, B., Hu, C., 2024. Comparison of perfluoroalkyl substance adsorption performance by inorganic and organic silicon modified activated carbon. Water Res. 260. https://doi.org/10.1016/j.watres.2024.121919.

Jjagwe, J., Olupot, P.W., Menya, E., Kalibbala, H.M., 2021. Synthesis and application of granular activated carbon from biomass waste materials for water treatment: a review. J. Bioresour. Bioprod. 6, 292–322. https://doi.org/10.1016/j.jobab.2021.03.003.

Juve, J.-M.A., Donoso Reece, J.A., Wong, M.S., Wei, Z., Ateia, M., 2024. Photocatalysts for chemical-free PFOA degradation – what we know and where we go from here? J. Hazard. Mater. 462. https://doi.org/10.1016/j.jhazmat.2023.132651.

Kalinke, I., Pusl, F., Häderle, F., Kulozik, U., 2023. A comparative study of frequency-shifting strategies for uniform and energy-efficient microwave heating in solid-state microwave systems. Innov. Food Sci. Emerg. Technol. 86. https://doi.org/10.1016/j.ifset.2023.103388.

Kangani, A.A., Jafari, D., Esfandyari, M., Mahdavi, M., 2024. Transesterification of mustard oil to biodiesel using activated carbon/Fe2(MoO4)3/K2CO3 as a novel heterogeneous nanocatalyst: Box-Behnken design-based optimization and Gaussian process regression. Process. Saf. Environ. Prot. 189, 102–114. https://doi.org/10.1016/j.psep.2024.06.058.

Khedri, A., Jafari, D., Esfandyari, M., 2022. Adsorption of nickel(II) ions from synthetic wastewater using activated carbon prepared from mespilus germanica leaf. Arab. J. Sci. Eng. 47, 6155–6166. https://doi.org/10.1007/s13369-021-06014-7.

Lee, J., Kim, C., Liu, C., Wong, M.S., Cápiro, N.L., Pennell, K.D., Fortner, J.D., 2023. Ultra-high capacity, multifunctional nanoscale sorbents for PFOA and PFOS treatment. NPJ Clean. Water 6. https://doi.org/10.1038/s41545-023-00263-9.

Lee, T., Speth, T.F., Nadagouda, M.N., 2022. High-pressure membrane filtration processes for separation of Per- and polyfluoroalkyl substances (PFAS). Chem. Eng. J. 431. https://doi.org/10.1016/j.cej.2021.134023.

Lima, E.C., Sher, F., Guleria, A., Saeb, M.R., Anastopoulos, I., Tran, H.N., Hosseini-Bandegharaei, A., 2021. Is one performing the treatment data of adsorption kinetics correctly? J. Environ. Chem. Eng. 9, 104813. https://doi.org/10.1016/j.jece.2020.104813.

Liu, Zhiyuan, Yang, F., Zhai, T., Yu, J., Wang, C., Liu, Zhengang, Liu, Zhixue, Gao, Y., Yang, M., 2024. Removal of PFOA from water by activated carbon adsorption: Influence of pore structure. J. Environ. Chem. Eng. 12, 113923. https://doi.org/10.1016/j.jece.2024.113923.

Lonbar, M.M., Baghdadi, M., Mollasalehi, A., Pardakhti, A.R., 2025. Peroxydisulfate activation and singlet oxygen generation for effective bisphenol A removal from groundwater and treated wastewater by a novel NiO doped B2O3–porous carbon catalyst. Chem. Eng. J. Adv., 100907 https://doi.org/10.1016/j.ceja.2025.100907.

Ma, Q., Lei, Q., Liu, F., Song, Z., Khusid, B., Zhang, W., 2024. Evaluation of commercial nanofiltration and reverse osmosis membrane filtration to remove per-and polyfluoroalkyl substances (PFAS): Effects of transmembrane pressures and water matrices. Water Environ. Res. 96. https://doi.org/10.1002/wer.10983.

Mollasalehi, A., Baghdadi, M., Samiee-Zafarghandi, R., Lonbar, M.M., 2026. Sustainable metal–carbon composite derived from pharmaceutical waste: Using expired acetaminophen and aluminum ion precursors for photoreduction of Cr(VI) under visible light. Environ. Technol. Innov. 41, 104772. https://doi.org/10.1016/j.eti.2026.104772.

Nobakht, A., Jafari, D., Esfandyari, M., 2023. New insights on the adsorption of phenol red dyes from synthetic wastewater using activated carbon/Fe2(MoO4)3. Environ. Monit. Assess. 195, 574. https://doi.org/10.1007/s10661-023-11178-w.

Norouzi, H., Jafari, D., Esfandyari, M., 2020. Study on a new adsorbent for biosorption of cadmium ion from aqueous solution by activated carbon prepared from Ricinus communis. Desalin. Water Treat. 191, 140–152. https://doi.org/10.5004/dwt.2020.25702.

Pala, J., Le, T., Kasula, M., Rabbani Esfahani, M., 2023. Systematic investigation of PFOS adsorption from water by Metal Organic Frameworks, Activated Carbon, Metal Organic Framework@Activated Carbon, and functionalized Metal Organic Frameworks. Sep. Purif. Technol. 309, 123025. https://doi.org/10.1016/j.seppur.2022.123025.

Pauletto, P.S., Florent, M., Bandosz, T.J., 2022. Insight into the mechanism of perfluorooctanesulfonic acid adsorption on highly porous media: Sizes of hydrophobic pores and the extent of multilayer formation. Carbon 191, 535–545. https://doi.org/10.1016/j.carbon.2022.02.006.

Pauletto, P.S., Florent, M., Bandosz, T.J., 2023. On the directions of carbon surface modifications towards efficient PFOS removal: analyzing the interplay of porosity and surface chemistry. Chem. Eng. J. 455. https://doi.org/10.1016/j.cej.2022.140897.

Ranjbar, E., Ahmadi, F., Baghdadi, M., 2024. Regeneration of perfluorooctane sulfonic acid (PFOS) loaded granular activated carbon using organic/inorganic mixed solutions. Chem. Eng. Sci. 300, 120623. https://doi.org/10.1016/j.ces.2024.120623.

Shin, J., An, B., 2024. Effect of ligand interactions within modified granular activated carbon (GAC) on mixed perfluorooctanoic acid (PFOA) and perfluorooctanesulfonic acid (PFOS) adsorption. Chemosphere 357, 142025. https://doi.org/10.1016/j.chemosphere.2024.142025.

Taghizad, A., Kachoueiyan, F., Maleki Lonbar, M., Baghdadi, M., 2025. Highly efficient removal of perfluorooctanesulfonic acid (PFOS) from aqueous solutions at neutral pH using a novel and reusable porous Aluminum-Carbon composite (PACC). Environ. Technol. Innov. 40, 104623. https://doi.org/10.1016/j.eti.2025.104623.

Thue, P.S., Adebayo, M.A., Lima, E.C., Sieliechi, J.M., Machado, F.M., Dotto, G.L., Vaghetti, J.C.P., Dias, S.L.P., 2016. Preparation, characterization and application of microwave-assisted activated carbons from wood chips for removal of phenol from aqueous solution. J. Mol. Liq. 223, 1067–1080. https://doi.org/10.1016/j.molliq.2016.09.032.

Trzcinski, A.P., Harada, K.H., 2024. Comparison of perfluorooctane sulfonate (PFOS), perfluorooctanoic acid (PFOA) and perfluorobutane sulfonate (PFBS) removal in a combined adsorption and electrochemical oxidation process. Sci. Total. Environ. 927, 172184. https://doi.org/10.1016/j.scitotenv.2024.172184.

Vatankhah, G., Parsa, F., Jafari, D., Esfandyari, M., 2024. Evaluation of adsorptive performance of Mn-doped Fe2O4 nanoparticles loaded on activated carbon in removal of boron ions from synthetic wastewater. Biomass Convers. Biorefin 14, 26477–26487. https://doi.org/10.1007/s13399-023-04695-8.

Wu, H., Lu, Z., Hill, S., Turner, R., 2025. Microstructure characterisation and modelling of pre-forging solution treatment of 7075 aluminium alloy using novel heating methods. J. Manuf. Mater. Process. 9. https://doi.org/10.3390/jmmp9010002.

Yang, I., Jung, M., Kim, M.-S., Choi, D., Jung, J.C., 2021. Physical and chemical activation mechanisms of carbon materials based on the microdomain model. J. Mater. Chem. A Mater. 9, 9815–9825. https://doi.org/10.1039/D1TA00765C.

Yang, X., Song, C., Ren, M., Kong, Y., Cui, X., 2025. Distribution patterns and influencing factors of PFAS in soils: a meta-analysis. Environ. Res. 279. https://doi.org/10.1016/j.envres.2025.121806.

Yavari, M.A., Pishnamaz, H.M.N., Baghdadi, M., Abdoli, M.A., 2025. Perfluorooctanesulfonic acid (PFOS) removal from aqueous solution through N-doped porous copper-carbon composite derived from recycled copper obtained from fly ash incinerator: water decontamination via municipal waste remnants. Chemosphere 370, 143963.

Zahed, M., Jafari, D., Esfandyari, M., 2022. Adsorption of formaldehyde from aqueous solution using activated carbon prepared from *Hibiscus rosa-sinensis*. Int. J. Environ. Anal. Chem. 102, 2979–3001. https://doi.org/10.1080/03067319.2020.1762872.

Zakaria, A.F., Kamaruzaman, S., Abdul Rahman, N., Yahaya, N., 2023. Sodium alginate immobilized β-cyclodextrin/multi-walled carbon nanotubes as hybrid hydrogel adsorbent for perfluorinated compounds removal. J. Polym. Environ. 31, 1895–1914. https://doi.org/10.1007/s10924-022-02737-2.

Zhang, J., 2019. Physical insights into kinetic models of adsorption. Sep. Purif. Technol. 229, 115832. https://doi.org/10.1016/j.seppur.2019.115832.

Zhang, L., Si, C., Zeng, F., Duan, X., Zhang, D., Xu, W., Shi, J., 2024. Persulfate activation for efficient remediation of perfluorooctanoic acid (PFOA) and perfluorooctane sulfonic acid (PFOS) in water: Mechanisms, removal efficiency, and future prospects. J. Environ. Chem. Eng. 12. https://doi.org/10.1016/j.jece.2023.111422.

Zhang, Y., Tan, X., Lu, R., Tang, Y., Qie, H., Huang, Z., Zhao, J., Cui, J., Yang, W., Lin, A., 2023. Enhanced removal of polyfluoroalkyl substances by simple modified biochar: adsorption performance and theoretical calculation. ACS ES T Water 3, 817–826. https://doi.org/10.1021/acsestwater.2c00597.

Zhang, Y., Zhu, X., Li, X., Chen, B., 2021. situ quantitative determination of the intermolecular attraction between amines and a graphene surface using atomic force microscopy. J. Colloid Interface Sci. 581, 385–395. https://doi.org/10.1016/j.jcis.2020.07.112.